Fast decomposition of two ultrasound longitudinal waves in cancellous bone using a phase rotation parameter for bone quality assessment: Simulation study

Hirofumi Taki[a)]
Graduate School of Biomedical Engineering, Tohoku University, Sendai 980-8575, Japan

Yoshiki Nagatani
Department of Electronics, Kobe City College of Technology, Kobe 651-2194, Japan

Mami Matsukawa
Faculty of Science and Engineering, Doshisha University, Kyotanabe 610-0321, Japan

Hiroshi Kanai
Graduate School of Engineering, Tohoku University, Sendai 980-8579, Japan

Shin-Ichi Izumi
Graduate School of Biomedical Engineering, Tohoku University, Sendai 980-8575, Japan

(Received 3 May 2017; revised 31 August 2017; accepted 6 October 2017; published online 24 October 2017)

Ultrasound signals that pass through cancellous bone may be considered to consist of two longitudinal waves, which are called fast and slow waves. Accurate decomposition of these fast and slow waves is considered to be highly beneficial in determination of the characteristics of cancellous bone. In the present study, a fast decomposition method using a wave transfer function with a phase rotation parameter was applied to received signals that have passed through bovine bone specimens with various bone volume to total volume (BV/TV) ratios in a simulation study, where the elastic finite-difference time-domain method is used and the ultrasound wave propagated parallel to the bone axes. The proposed method succeeded to decompose both fast and slow waves accurately; the normalized residual intensity was less than −19.5 dB when the specimen thickness ranged from 4 to 7 mm and the BV/TV value ranged from 0.144 to 0.226. There was a strong relationship between the phase rotation value and the BV/TV value. The ratio of the peak envelope amplitude of the decomposed fast wave to that of the slow wave increased monotonically with increasing BV/TV ratio, indicating the high performance of the proposed method in estimation of the BV/TV value in cancellous bone. https://doi.org/10.1121/1.5008502

[KAW] Pages: 2322–2331

I. INTRODUCTION

Bone strength is known to depend on not only bone quantity (bone mineral density), but also "bone quality" which would be determined by several factors: microstructure, elasticity, and metabolism of bone. The gold standard method for diagnosis of osteoporosis is dual x-ray absorptiometry. However, because this method measures the bone mineral density only, its performance in the estimation of osteoporosis is limited (Genant and Jiang, 2006; Blake and Fogelman, 2007). Quantitative ultrasound (QUS) is another modality that is used to evaluate bone quality by estimating the speed of sound and the broadband ultrasonic attenuation characteristics of the bone (Langton *et al.*, 1984; Laugier, 2008; Barkmann *et al.*, 2008; Bouxsein *et al.*, 1995; Njeh *et al.*, 1997; Han *et al.*, 1997; Lochmüller *et al.*, 1999; Haïat *et al.*, 2009). It may be considered that ultrasound signals passing through cancellous bone consist of two longitudinal waves, which are called fast and slow waves (Hosokawa and Otani, 1997, 1998; Hosokawa, 2010; Mizuno *et al.*, 2008; Mizuno *et al.*, 2009; Haïat *et al.*, 2008; Padilla and Laugier, 2000). Because the fast wave mainly propagates through the bone trabeculae, the properties of the wave reflect the structure of the cancellous bone (Hosokawa and Otani, 1997, Mizuno *et al.*, 2008; Mizuno *et al.*, 2010). In addition, another previous work reported that the amplitude of the slow wave is closely related to the bone volume (Otani 2005). Therefore, analysis of these two waves should reveal both the state of the cancellous structure of the bone and the bone volume, which are useful in the evaluation of bone quality (Cardoso *et al.*, 2003; Haïat *et al.*, 2007; Hosokawa 2009; Laugier and Haïat, 2011). However, the fast and slow waves overlap with each other in many cases, thus obstructing accurate analysis of the properties of the two waves.

Accurate decomposition of the fast and slow waves would be highly beneficial for determination of the characteristics of cancellous bone. One strategy that has been used to decompose these waves is application of a Bayesian method that uses a Markov chain Monte Carlo method with simulated annealing (Marutyan *et al.*, 2007; Anderson *et al.*, 2010; Nelson *et al.*, 2011; Hoffman *et al.*, 2012; Groopman *et al.*, 2015). The Bayesian decomposition method has

a)Electronic mail: hirofumi.taki.a1@tohoku.ac.jp

demonstrated high performance in accurately characterizing the fast and slow waves, but at the cost of a high computational load. Two other approaches that have been used are fast decomposition algorithms: the modified least-square Prony method and the space-alternating generalized expectation-maximization algorithm (Dencks and Schmitz 2013; Wear 2013, 2014). The Bayesian and the modified least-square Prony methods yielded comparable results for the ultrasonic properties of fast and slow waves in cancellous bone; however, additional improvement in decomposition performance is desirable.

We recently reported a fast decomposition method that was based on a minimum variance (MV) range beamformer, called the MV beamformer for range resolution improvement (Taki *et al.*, 2015). The method introduces a modified wave transfer function with a phase rotation parameter that can compensate for the arrival time distribution that is caused by path-length variations within a bone specimen. The fast decomposition method has demonstrated high accuracy in characterization of the two waves on a similar level to that of a Bayesian method, thus indicating the validity of use of the modified wave transfer function with the phase rotation parameter.

In the present study, we investigated the relationship between the two decomposed waves and the bone volume using the above method to evaluate the performance of the decomposition method for bone quality assessment. A previous study reported that the waveform of the ultrasound signal changed not only with the bone sample thickness but also with the transducer size (Fujita *et al.*, 2013). Therefore, we applied the fast decomposition method with the modified wave transfer function to received signals that had passed through bone specimens with various bone volume to total volume (BV/TV) ratios and transducer sizes in a simulation study using the finite-difference time-domain (FDTD) method, in which the bone sample was fully immersed in water. The aims of the study can be considered to be twofold. First, we investigated the validity of the phase rotation parameter that was used by the modified wave transfer function. Second, we evaluated the performance of the proposed fast decomposition method with the modified wave transfer function in estimation of the porosity of cancellous bone.

II. METHODS

The fast decomposition method uses a modified transfer function with a phase rotation parameter. In this section, we explain the simulation settings used to construct the received signals that pass through bone specimens with various BV/TV values and transducer sizes. We then briefly describe the modified transfer function and the decomposition strategy that was reported in our previous work (Taki *et al.*, 2015).

A. Simulation settings

To derive the signals of samples with various BV/TV values, the elastic FDTD method was used. The FDTD simulation software was originally programmed by our group (Nagatani *et al.*, 2006). For the FDTD simulations, a parallelepipedic bovine cancellous bone sample was used (Nagatani *et al.*, 2008). Three-dimensional bone models were created using x-ray micro-focus computed tomography (x-ray μCT) images (SMX-100CT, Shimadzu, Kyoto, Japan) of an actual bone sample. The spatial resolution of the CT images was 46.0 μm. Because the CT images are grayscale images, the simulation models were created by selecting a specific binarization threshold that determines the trabecular thickness but does not influence the bone structure (Nagatani and Tachibana, 2014). In this case, seven thresholds of 145, 146, 147, 148, 149, 150, and 151 on a 256-scale gray image were selected, which meant that the BV/TV ratios of the constructed models ranged from 0.144 to 0.226. Figure 1 shows the bone structure under the seven BV/TV conditions. The bone model dimensions were $15 \times 15 \times 8\,\mathrm{mm}^3$ and the simulation field dimensions were $16 \times 16 \times 13\,\mathrm{mm}^3$. To investigate the gradual change of the waveform as it propagated inside the cancellous bone, the model was gradually reduced in thickness from 8 to 4 mm at intervals of 1 mm. The porous part of the cancellous bone was filled with water. The experimental observed values for wave speed and attenuation in the bovine cortical bone were used for the trabecular part of the cancellous bone (Sasso *et al.*, 2007, 2008; Yamato *et al.*, 2008; Yamamoto *et al.*, 2008; Nagatani and Tachibana, 2014). The parameters that were used in the simulations are shown in Table I. As the initial signal at the surface of the plane source, an experimentally observed

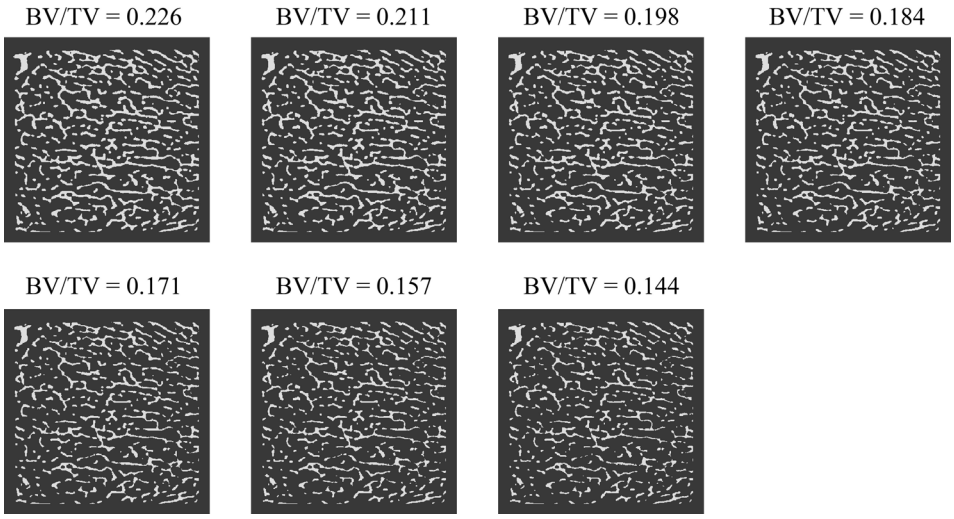

FIG. 1. Bone specimen structure used in the simulation study.

TABLE I. Parameters used in the FDTD simulations.

Material		Water	Trabecular bone
Density [g/cm^3]		1.0	2.0
Velocity [m/s]	Longitudinal wave	1483	4060
	Shear wave	-	2450

waveform of a single sinusoidal sound wave at a frequency of 1 MHz that passed through the water was used. The wave propagation direction was parallel to the direction of the predominant bone axis. The received signal was then calculated at the plane surface that was placed opposite the transmitter, where the size of the receiving transducer was same as that of the transmitting transducer. In the present study, we used four different sizes of transducers, 40%, 60%, 80%, and full-size of the simulation field size, that is, we used square transducers with side lengths of 6.4, 9.7, 12.9, and 16 mm.

B. Modified wave transfer functions for fast and slow waves

The modified wave transfer functions for the fast and slow waves are based on the wave transfer function that was modeled for waves passing through cancellous bone in previous studies (Marutyan *et al.*, 2006; Anderson *et al.*, 2008). The propagation models are expressed using the following formula:

$$S_{\mathrm{R}}(f) = S_{\mathrm{I}}(f)[H_1(f) + H_2(f)], \tag{1}$$

where $S_{\mathrm{R}}(f)$ is a frequency component of the received signal passing through a bone specimen in water at a frequency f, $S_{\mathrm{I}}(f)$ is the same component passing through a water-only path, and $H_1(f)$ and $H_2(f)$ are the transfer functions for the fast and slow waves, respectively.

Several researchers have introduced the assumption that the wavefront of an ultrasound wave passing through a bone specimen in water is the same as that passing through water-only pass. However, during ultrasound propagation through cancellous bone, there will be multiple paths with various path lengths, causing an uneven wavefront and complicated changes in the waveform. Because the ultrasound waves that pass through these multiple paths of various lengths are typically received by a flat transducer, the path-length-variation (PLV) should affect the transfer function. The modified wave transfer function approximates this effect using the following formula:

$$S_{\mathrm{R}}{}'(f) = S_{\mathrm{I}}(f)[F_{\mathrm{T1}}(f)H_1(f) + F_{\mathrm{T2}}(f)H_2(f)], \tag{2}$$

$$F_{\mathrm{T}i}(f) \cong A_{\mathrm{T}i}\exp[-\gamma_i f + \mathrm{j}(\delta_i f + \theta_i)], \tag{3}$$

where $F_{\mathrm{T1}}(f)$ and $F_{\mathrm{T2}}(f)$ are the frequency components for the fast and slow waves, respectively, that originate from the PLV effect, and $A_{\mathrm{T}i}$, γ_i, δ_i, and θ_i are real constants. $\gamma_i f$ and $\mathrm{j}\delta_i f$ denote the attenuation and the time shift, respectively. θ_i is a phase rotation parameter that is independent of f. In a linear-with-frequency attenuation model, the modified wave transfer function that accounts for the PLV effect is expressed using the following formula (Taki *et al.*, 2015):

$$\begin{aligned} H_i'(f) &= F_{\mathrm{T}i}(f)H_i(f) \\ &= A_i'\exp\left[-\beta_i' fd + \mathrm{j}\left\{\frac{2\pi fd}{c_i(f)} - \frac{2\pi fd}{c_{\mathrm{W}}}\right\} + \mathrm{j}\delta_i f + \mathrm{j}\theta_i\right], \end{aligned} \tag{4}$$

$$A_i' = A_i A_{\mathrm{T}i}, \tag{5}$$

$$\beta_i' = \beta_i + \frac{\gamma_i}{d}, \tag{6}$$

where A_i is a signal amplitude parameter that is independent of f, β_i is the attenuation coefficient, d is the bone specimen thickness, $c_i(f)$ is the phase velocity, and c_{W} is the sound velocity in water. For each specimen with constant thickness d, $A_{i,}'$ and β_i' are real constants, and $\mathrm{j}\delta_i f$ denotes the time shift. When the phase velocities of the two waves satisfy the Kramers-Kronig relations, they can be expressed using the following formula (Waters *et al.*, 2005; Bauer *et al.*, 2007; O'Donnell *et al.*, 1978):

$$\frac{1}{c_i(f)} - \frac{1}{c_i(f_0)} = -\frac{\beta_i}{\pi^2}\ln\left(\frac{f}{f_0}\right), \tag{7}$$

where f_0 is a reference frequency.

C. Fast deconvolution method based on MV range beamformer

The fast deconvolution method consists of two steps: the first step estimates the rise times of the fast and slow waves using the MV range beamformer, and the second step decomposes these two waves using the least squares method in the time domain.

1. Rise time estimation using the MV range beamformer

During estimation of the fast wave, it is preferable to select a time window in which the contribution of the slow wave is negligible. To determine the appropriate time window for characterization of the fast wave, the decomposition method estimates the slow wave rise time using the MV range beamformer with frequency domain interferometry.

We prepared multiple candidate waves for use as the fast and slow waves using the modified wave transfer function. The MV range beamformer uses each of the candidate waves as a reference wave, and it then calculates the rise time and the estimated intensity for each candidate wave separately. The received signal is then normalized using a reference signal to adjust the intensities and phases of all frequency components uniformly (Taki *et al.*, 2012; Taki *et al.*, 2015):

$$X_{\mathrm{H}l} = X_l X_{\mathrm{R}l}{}^*/(|X_{\mathrm{R}l}|^2 + \eta), \tag{8}$$

where X_l, $X_{\mathrm{H}l}$, and $X_{\mathrm{R}l}$ are the lth frequency components of the received signal, of the received signal after normalization, and of the reference signal, respectively; the superscript []* denotes a complex conjugate, and η is a constant term that is used for

stabilization. Because the optimum filter is the Wiener filter, the optimum value of eta should be equal to the noise intensity for each frequency component. When the signal intensity is constant and only white noise exists, we can estimate the noise intensity of each frequency component using the variance expectation of the intensity of the component. However, in medical ultrasound imaging, the signal intensity is commonly variable and speckle is signal correlated noise. In the present study, we followed our previous study (Taki *et al.*, 2015) and introduced the assumption that the expectation of the noise intensity is 40 dB lower than the average intensity of the reference signal, that is, η was set to be 40 dB lower than the average intensity of the reference signal $X_{\mathrm{R}l}$.

The MV range beamformer minimizes the output intensity under the constraint of a constant response for the reference signal at a specific measurement depth (Taki *et al.*, 2012). This problem can be expressed using the following formulae:

$$\min \quad \mathbf{W}^{\mathrm{T}^*}\mathbf{R}_{\mathrm{A}}\mathbf{W} \quad \text{subject} \quad \text{to} \quad \mathbf{C}^{\mathrm{T}^*}\mathbf{W} = 1\,, \tag{9}$$

$$\mathbf{R}_{\mathrm{A}} = \frac{1}{M}\sum_{m=1}^{M}\mathbf{X}_m\mathbf{X}_m^{\mathrm{T}^*}, \tag{10}$$

$$\begin{aligned}\mathbf{X}_m &= \left[X_{\mathrm{H}m} \quad X_{\mathrm{H}(m+1)} \quad \cdots \quad X_{\mathrm{H}(m+L-1)}\right]^{\mathrm{T}},\\ \mathbf{C} &= \left[\mathrm{e}^{\mathrm{j}\omega_1 t} \quad \mathrm{e}^{\mathrm{j}\omega_2 t} \quad \cdots \quad \mathrm{e}^{\mathrm{j}\omega_L t}\right]^{\mathrm{T}},\end{aligned} \tag{11}$$

where $\mathbf{R}_{\mathrm{A}}$ is the covariance matrix of the normalized frequency components after frequency averaging, $\mathbf{W}$ is a weighting vector, ω_l is the lth angular frequency, L is the size of $\mathbf{R}_{\mathrm{A}}$, and M is the number of sub-matrices that were used for frequency averaging. The estimated intensity using the optimum weighting vector can be expressed as

$$P_{\mathrm{MVR}}(t) = \frac{1}{\mathbf{C}^{\mathrm{T}^*}(\mathbf{R}_{\mathrm{A}} + \eta'\mathbf{E})^{-1}\mathbf{C}}, \tag{12}$$

where $\eta'\mathbf{E}$ is a diagonal loading that was used for stabilization. In the present study, the value of η' was set to be 40 dB lower than the average value of the diagonal elements of $\mathbf{R}_{\mathrm{A}}$. The size of M is set to be 40% of the total number of frequency components.

We calculate the intensity profiles $P_{\mathrm{MVR}}(t)$ for all the candidate reference waves for the slow waves, and then select the time at which the intensity is the highest among all the candidates. The selected time is the tentative rise time of the slow wave T_{S}. The decomposition procedure of the fast wave using the least squares method uses the received signal at which $t < T_{\mathrm{S}}$ to eliminate the slow wave's contribution. We prepared 11 candidate reference waves for each of the fast and slow waves, where the thickness d in Eq. (4) ranged from 5 to 25 mm with a sampling interval of 2 mm. We used candidates with peak intensities that were higher than 1/100 of the maximum peak intensity for the fitting procedure using the least squares method.

2. Decomposition using the least squares method

The proposed decomposition method uses the least squares method in the time domain (Taki *et al.*, 2015). To suppress the computational complexity of the process, we modify the wave transfer function of Eq. (4) using propagation parameters that were reported in a previous study, as described below. The wave transfer function used in the decomposition process is given by

$$\begin{aligned}H_i'(f) \cong A_i' \exp\Bigg[&-\beta_{\mathrm{P}i} f d_{\mathrm{T}i} + \mathrm{j}\left\{\frac{2\pi f d_{\mathrm{T}i}}{c_{\mathrm{P}i}(f)} - \frac{2\pi f d_{\mathrm{T}i}}{c_{\mathrm{W}}}\right\}\\ &+\mathrm{j}\delta_i' f + \mathrm{j}\theta_i'\Bigg],\end{aligned} \tag{13}$$

$$\frac{1}{c_{\mathrm{P}i}(f)} - \frac{1}{c_i(f_0)} = -\frac{\beta_{\mathrm{P}i}}{\pi^2}\ln\left(\frac{f}{f_0}\right), \tag{14}$$

where $d_{\mathrm{T}i}$ is the temporal specimen thickness, and $\beta_{\mathrm{P}i}f$ and $c_{\mathrm{P}i}(f)$ are the provisional attenuation coefficient and phase velocity that were reported in the previous study (Nelson *et al.*, 2011). The proposed method optimizes the following four parameters for each wave: the signal amplitude parameter A_i', the temporal specimen thickness $d_{\mathrm{T}i}$, the time shift parameter δ_i', and the phase rotation θ_i'. Because the proposed method characterizes each wave alternately, the four parameters are all estimated simultaneously.

When the rise time $T_{\mathrm{R}i} = 0$, candidates for the fast and slow waves in the time domain are expressed using the following formulae:

$$\begin{aligned}s_i(d_{\mathrm{T}i}, A_i', \theta_i', t) &= \mathrm{Re}\left\{F^{-1}\left[S_{\mathrm{I}}(f)H_i'(f)_{T_{\mathrm{R}i}=0}\right]\right\}\\ &\cong A_i'\cos\theta_i'\mathrm{Re}\{s_i'(t)\}\\ &\quad + A_i'\sin\theta_i'\mathrm{Re}\{\mathrm{j}s_i'(t)\},\end{aligned} \tag{15}$$

$$\begin{aligned}s_i'(t) = \mathbf{F}^{-1}\Bigg(S_{\mathrm{I}}(f)\exp\Bigg[&-\beta_{\mathrm{P}i} f d_{\mathrm{T}i} + \mathrm{j}\left\{\frac{2\pi f d_{\mathrm{T}i}}{c_{\mathrm{P}i}(f)}\right.\\ &\left.-\frac{2\pi f d_{\mathrm{T}i}}{c_{\mathrm{W}}}\right\} + \mathrm{j}\delta_i'' f\Bigg]\Bigg),\end{aligned} \tag{16}$$

where $\mathbf{F}^{-1}$ denotes an inverse Fourier transform. δ_i'' is used in the setting of $T_{\mathrm{R}i} = 0$. We prepare $s_i'(t)$ for all candidate waves in advance for use by the proposed method in the decomposition process.

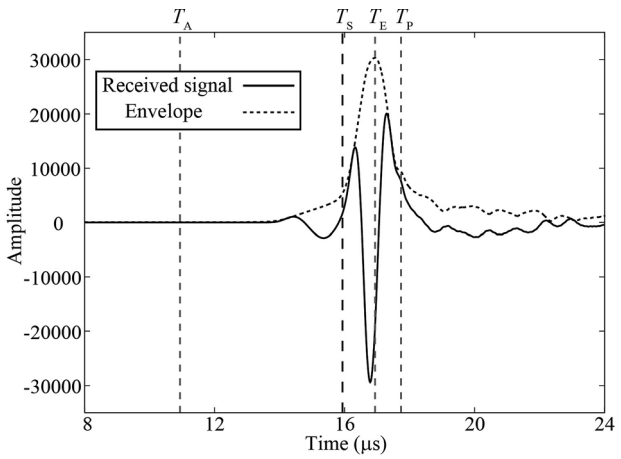

FIG. 2. Fitting region used in decomposition of fast and slow waves using the least squares method. T_{E} is the peak time of the envelope, and T_{S} is the rise time of the slow wave that was calculated using the frequency domain interferometry (FDI) imaging method. $T_{\mathrm{A}} = T_{\mathrm{E}} - 6\,\mu$s, and $T_{\mathrm{P}} = T_{\mathrm{E}} + 0.8\,\mu$s.

The proposed method characterizes the fast and slow waves alternately based on minimization of the sum of squares D of four variables:

$$D(d_{\mathrm{T}i},A_i',\theta_i',T_{\mathrm{R}i})=\sum_{t=T_1}^{T_2}|s_{\mathrm{o}}(t)-s_i(d_{\mathrm{T}i},A_i',\theta_i',t-T_{\mathrm{R}i})|^2, \quad (17)$$

where $s_{\mathrm{o}}(t)$ is the objective function used for the fitting, and $T_1 \le t \le T_2$ is the fitting region. Because $A_i'\cos\theta_i'$ and $A_i'\sin\theta_i'$ are real numbers, the estimation of A_i' and θ_i' only requires a single linear least squares process. Therefore, the required number of linear least squares processes is given by the product of the number of candidate specimen

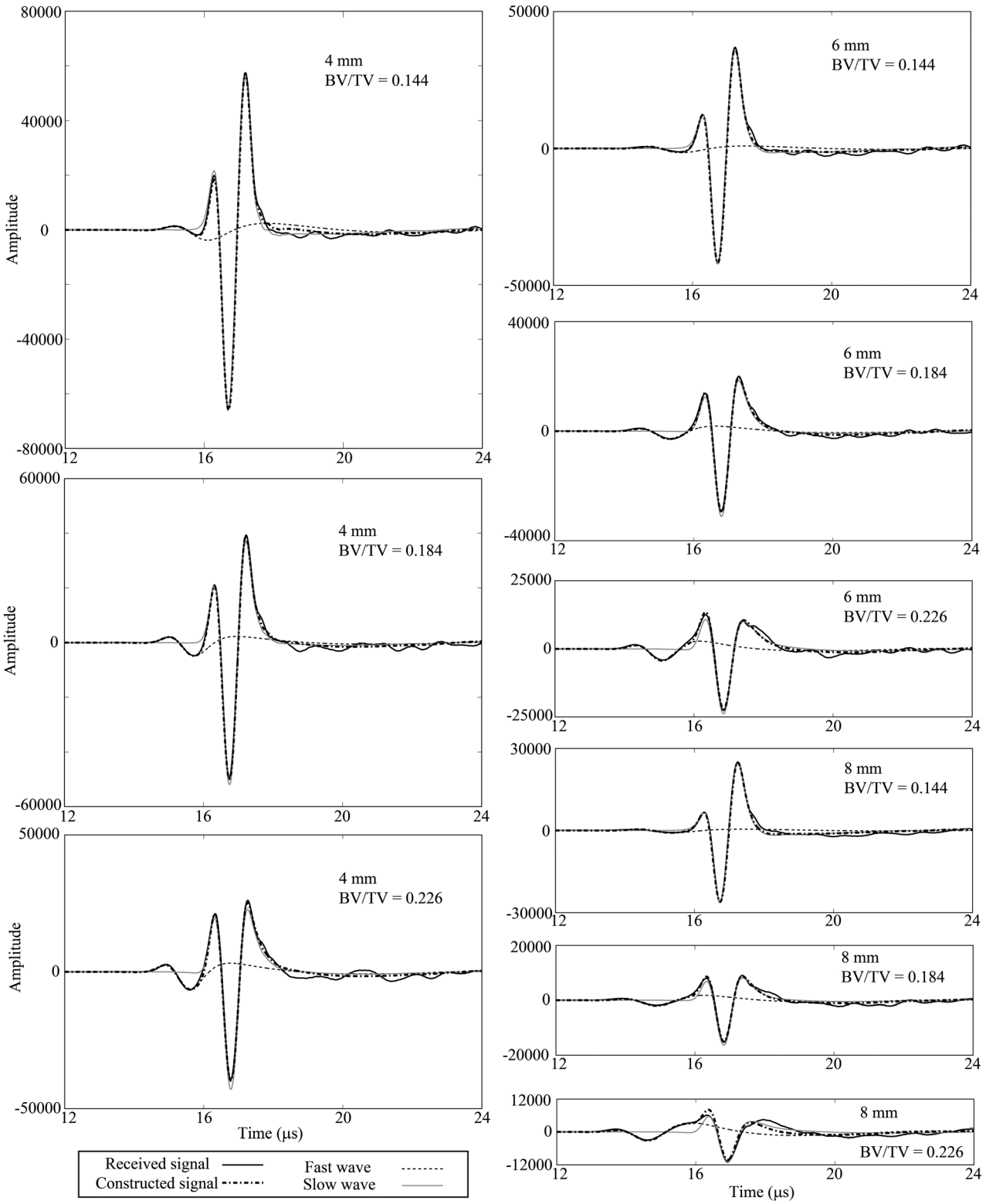

FIG. 3. Fast and slow waves that were estimated using the proposed decomposition method for specimen thicknesses of 4, 6, and 8 mm in the simulation study. Each constructed signal represents the summation of the estimated fast and slow waves, where the bone volume to total volume (BV/TV) ratio ranged from 0.144 to 0.226 and the transducer size was 16 mm.

thicknesses d_{Ti} and the number of candidate rise times T_{Ri}. The objective function $s_o(t)$ for the fast and slow waves is expressed using

$$s_o(t) = \begin{cases} s_R(t) - s_{E2}(t) & \text{(fast wave)}, \\ s_R(t) - s_{E1}(t) & \text{(slow wave)}, \end{cases} \quad (18)$$

where $s_R(t)$ is the received signal in the time domain, and $s_{E1}(t)$ and $s_{E2}(t)$ are the fast and slow waves that were estimated using the previous least mean squares process, respectively.

We prepared 111 candidates for each of the fast and slow waves, where d ranged from 4 to 26 mm using a sampling interval of 0.2 mm. The candidate rise times ranged from $T_{iMVR} - 0.8\,\mu$s to $T_{iMVR} + 0.8\,\mu$s for the fast and slow waves, where T_{iMVR} is the rise time that was calculated using the MV range beamformer. Figure 2 shows the fitting region that was used in the decomposition process using the least squares method. The fitting region in the present study ranged from $T_A = T_E - 6\,\mu$s to $T_P = T_E + 0.8\,\mu$s, where T_E is the peak time of the envelope. We followed our previous study to set these parameters (Taki *et al.*, 2015). The $t < T_A$ region contains almost no signal. In the region where $t > T_P$, the contributions of multiple reflections in the cancellous bone might not be negligible. First, the proposed method characterizes the slow wave using the received data within a fitting region of $T_S \le t \le T_P$, because the slow wave rise time should be close to the rise time T_S that was estimated using the MV range beamformer. During the fast wave characterization, the proposed method uses the received data within a fitting region of $T_A \le t \le T_S$ to eliminate the contribution of the slow wave. Following characterization of the fast wave, the proposed method characterizes the slow wave using the received data from the whole fitting region, represented by $T_A \le t \le T_P$.

III. RESULTS

Figure 3 shows the fast and slow waves that were decomposed using the proposed method, where the BV/TV ratio ranged from 0.144 to 0.226 and the transducer size was 16 mm (Nagatani and Tachibara, 2014). The signals that were constructed by the summation of the decomposed fast and slow waves agreed strongly with the received signals. Figure 4 shows the residual intensity when normalized with respect to the received signal intensity over the fitting region. The normalized residual intensity was less than −19.5 dB, except under the conditions where the specimen thickness was 8 mm and the BV/TV ratio was 0.211 or more. Figure 5 shows the fast and slow waves that were decomposed using the proposed method, where the BV/TV ratio was 0.184 and the transducer size ranged from 6.4 to 12.9 mm. Figure 6 shows the residual intensity when normalized with respect to the received signal intensity over the fitting region, where the normalized residual intensity was less than −22.7 dB. These results demonstrate the excellent performance of the proposed method in decomposition of the fast and slow waves. The decomposition of two waves requires 5.5 s using a Laptop PC with a single central processing unit (CPU).

Figure 7 shows the peak amplitudes of the envelopes of the fast and slow waves that were decomposed by the proposed method, where the BV/TV ratio ranged from 0.144 to 0.226 and the transducer size was 16 mm. The amplitude of the fast wave envelope increased as the BV/TV value increased; in contrast, that of the slow wave decreased under

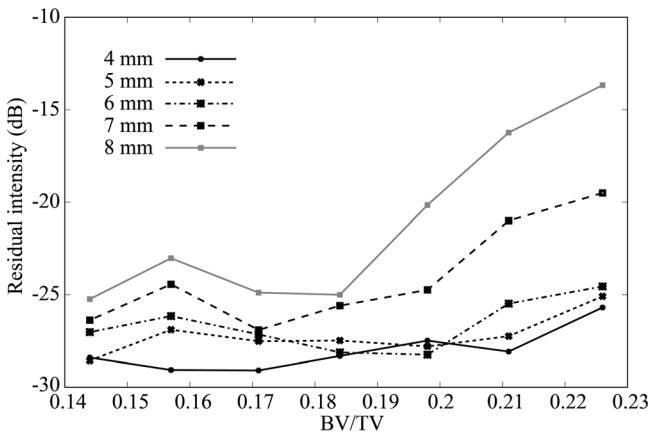

FIG. 4. Residual intensity normalized with respect to the received signal intensity over the fitting region for specimen thicknesses ranging from 4 to 8 mm, where the BV/TV ratio ranged from 0.144 to 0.226 and the transducer size was 16 mm.

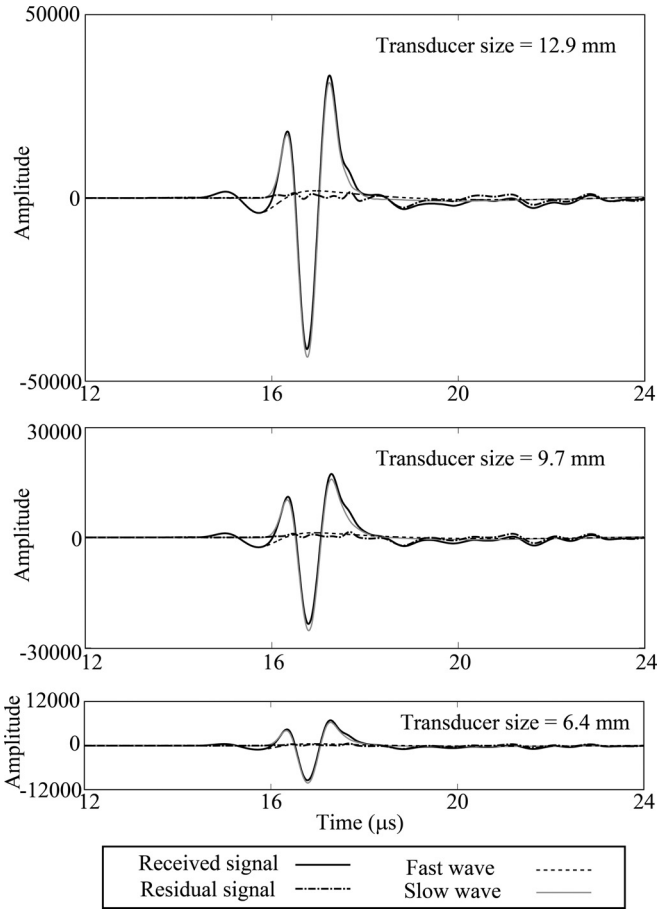

FIG. 5. Fast and slow waves that were estimated by the proposed decomposition method for a specimen thickness of 4 mm in the simulation study. Each residual signal was obtained by subtracting the estimated fast and slow waves from the received signal, where the BV/TV value was 0.184 and the transducer size ranged from 6.4 to 12.9 mm.

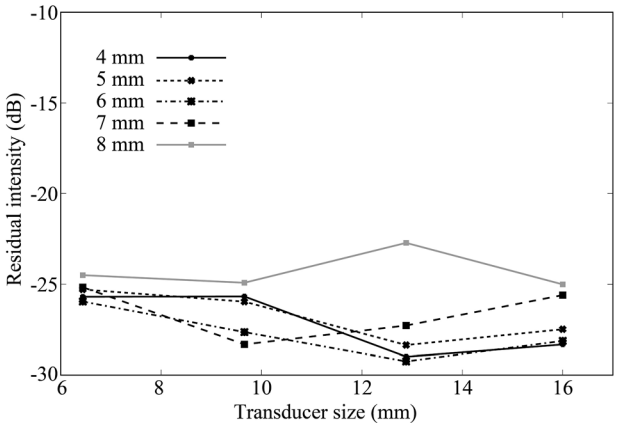

FIG. 6. Residual intensity when normalized with respect to the received signal intensity over the fitting region for specimen thicknesses ranging from 4 to 8 mm, where the BV/TV value was 0.184 and the transducer size ranged from 6.4 to 16 mm.

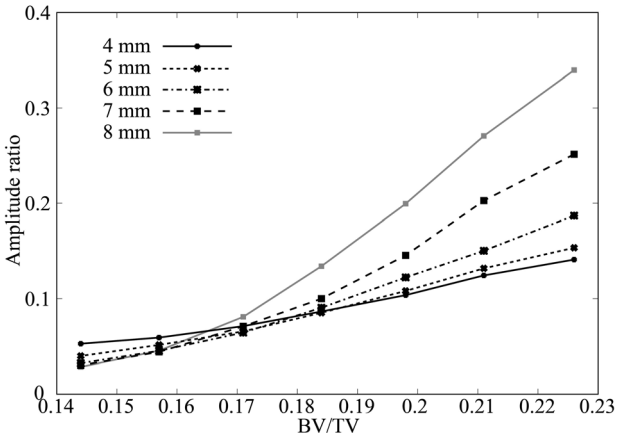

FIG. 8. Ratio of the peak envelope amplitude of the fast wave to that of the slow wave for specimen thicknesses ranging from 4 to 8 mm, where the BV/TV value ranged from 0.144 to 0.226 and the transducer size was 16 mm.

the same conditions. Therefore, the ratio of the peak envelope amplitude of the fast wave to that of the slow wave increases monotonically, as shown in Fig. 8. Because the increase in the BV/TV value indicates thicker trabeculae, this result is consistent with the consensus that the fast waves mainly propagate in the trabeculae. Figure 9 shows the ratio of the peak envelope amplitude of the fast wave to that of the slow wave, where the BV/TV ratio was 0.184 and the transducer size ranged from 6.4 to 16 mm. The amplitude ratio decreased as the transducer size increased from 6.4 to 16 mm; however, the observed variation was much smaller than that caused by a change in the BV/TV ratio from 0.144 to 0.226, and the amplitude ratio of BV/TV = 0.184 when using 6.4 mm transducers was close to that for BV/TV = 0.198 when using 16 mm transducers.

Figure 10 shows the phase rotation parameters for the fast and slow waves that were estimated by the proposed method, where the BV/TV ratio ranged from 0.144 to 0.226 and the transducer size was 16 mm. In both the fast and slow waves, the phase rotation variations with respect to BV/TV increased in magnitude with increasing bone specimen thickness. The phase rotation value of the estimated fast wave decreased as the BV/TV value increased. In contrast, the corresponding value of the slow wave increased. The large phase rotation values and small residual intensity shown in Fig. 4 illustrate the necessity of using the phase rotation parameter in the wave transfer function.

Figure 11 shows the phase rotation parameters for the fast and slow waves that were estimated by the proposed method, where the BV/TV ratio was 0.184 and the transducer size ranged from 6.4 to 16 mm. The phase rotation variation caused by the change in the transducer size was much smaller than that which was caused by changes in the BV/TV value. This result indicates the relationship that exists between the BV/TV ratio and the phase rotations of the two waves.

IV. DISCUSSION

This study employed an image processing algorithm to modify bone volume fraction by using the same x-ray μCT images of a sample (Haïat *et al.*, 2007; Nagatani *et al.*, 2017). The binarizing threshold applied to the original x-ray μCT images was varied so that the bone volume fraction of the model was varied. We should notice that, by changing

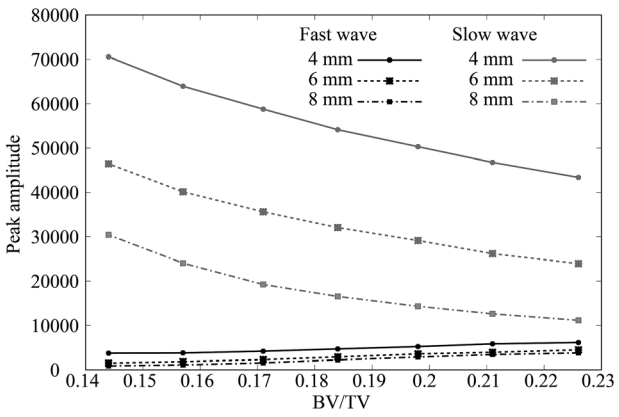

FIG. 7. Peak amplitudes of the envelopes of the fast and slow waves that were decomposed by the proposed method for specimen thicknesses ranging from 4 to 8 mm, where the BV/TV value ranged from 0.144 to 0.226 and the transducer size was 16 mm.

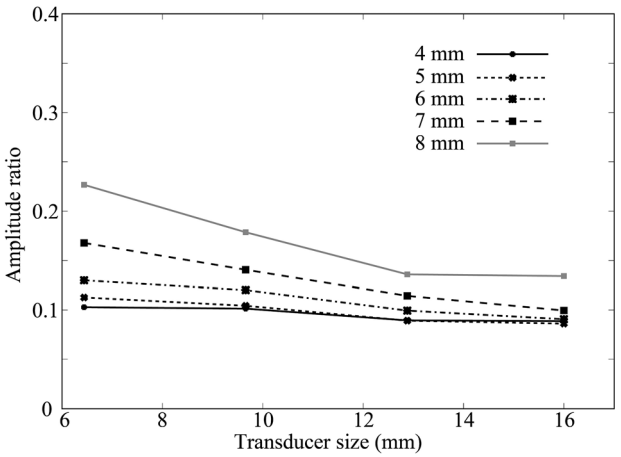

FIG. 9. Ratio of the peak envelope amplitude of the fast wave to that of the slow wave for specimen thicknesses ranging from 4 to 8 mm, where the BV/TV value was 0.184 and the transducer size ranged from 6.4 to 16 mm.

the threshold, the connectivity of the trabeculae might be slightly changed and the direction of the thickness change might not be exactly omnidirectional. This phenomenon can occur in the *in vivo* situation, e.g., osteoporosis. Future work should include the investigation of the limitation of this image processing algorithm.

The ratio of the peak envelope amplitude of the fast wave to that of the slow wave increased monotonically with increasing BV/TV, as shown in Fig. 8. The amplitude ratio increased as the transducer size decreased; however, a 40% reduction in the transducer size caused an increase in amplitude ratio similar to that caused by a 10% increase in BV/TV. Because the appearance of the two-wave phenomenon was reported in the case of waves passing through cancellous bone with cortical bone (Nagatani *et al.*, 2014), these results indicate that accurate decomposition of the fast and slow waves will enable precise estimation of the value of the BV/TV ratio in cancellous bone, and that the proposed decomposition method is highly promising as a novel technique for osteoporosis diagnosis using QUS.

Figure 10 shows the strong relationship that exists between the phase rotation value and the value of the BV/TV ratio, where variation of the phase rotation increases with increasing specimen thickness. The increase in the BV/TV value indicates thicker bone trabeculae in the cancellous bone, and the variation in the path length increases with increasing specimen thickness. Because both the increase in interaction through the surfaces of the bone trabeculae and the increase in the specimen thickness should lead to variation in the path length distribution, this result is consistent with the results of the method in which the phase rotation originates from the path length distribution. The phase rotation of the fast wave decreased as the value of BV/TV increased. In contrast, the phase rotation of the slow wave increased under the same conditions. This phenomenon may also have originated from the path-length variations.

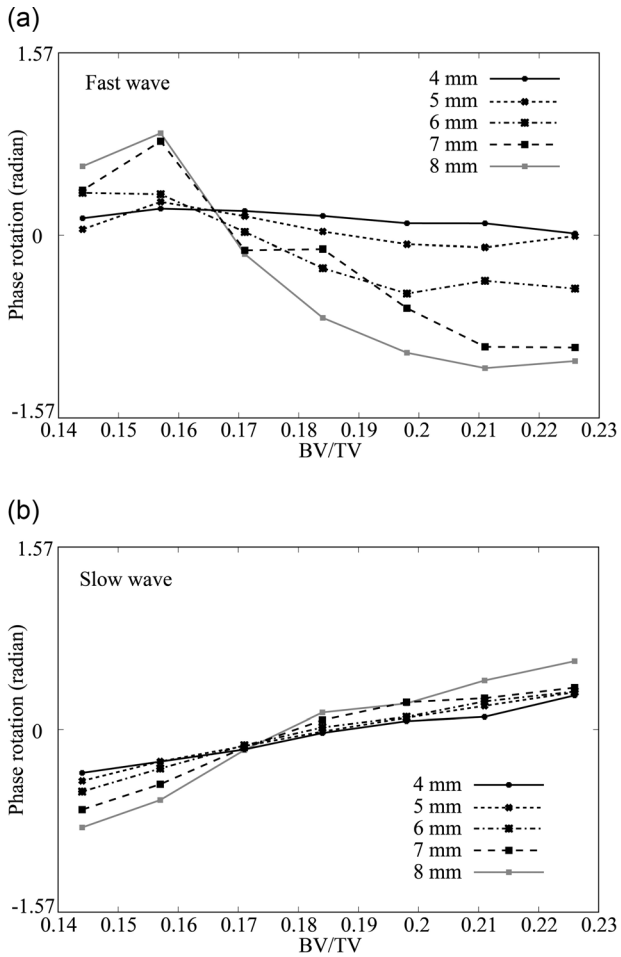

FIG. 10. Phase rotation parameters for (a) fast and (b) slow waves for specimen thicknesses ranging from 4 to 8 mm, where the BV/TV value ranged from 0.144 to 0.226 and the transducer size was 16 mm.

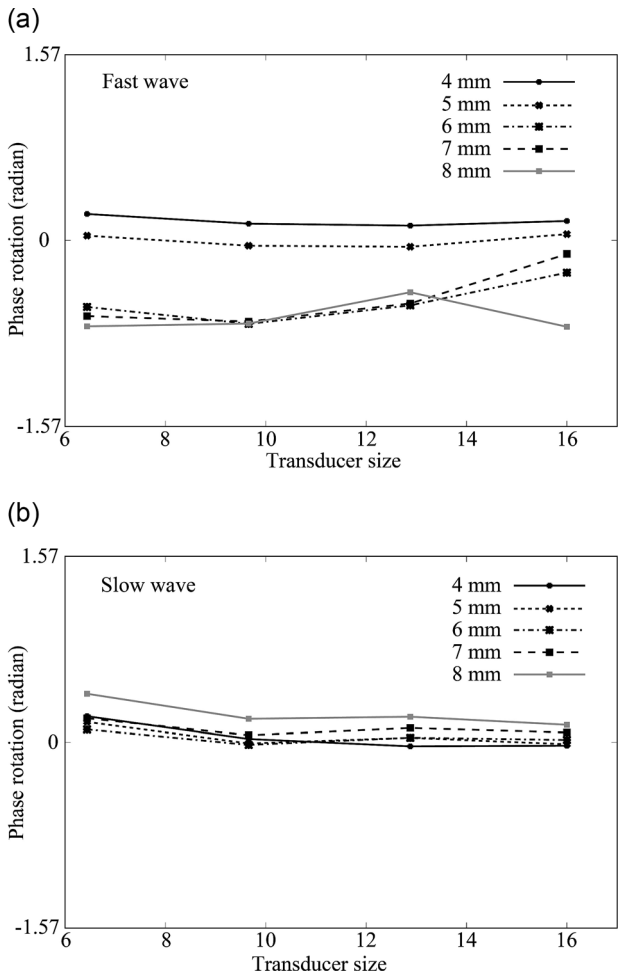

FIG. 11. Phase rotation parameters for (a) fast and (b) slow waves for specimen thicknesses ranging from 4 to 8 mm, where the BV/TV value was 0.184 and the transducer size ranged from 6.4 to 16 mm.

Both the amplitude ratio and the phase rotation were almost independent of the specimen thickness when the BV/TV ratio was approximately 0.17, as shown in Figs. 8 and 10. This phenomenon should be investigated in future work; however, it may simply be caused by the balance of the ultrasound signals that pass through the trabecular surface. When the contribution of the ultrasound that goes from the trabecular bone to the bone marrow is equivalent to that from the bone marrow to the trabecular bone at each frequency, the contributions of the ultrasound signals that pass through the trabecular surface may be negligible, thus suppressing the effects of the specimen thickness on the signal waveform.

V. CONCLUSION

In the present study, we apply a fast decomposition method that uses the wave transfer function with a phase rotation parameter to received signals that have passed through bone specimens with various BV/TV values in a simulation study. The normalized residual intensity was less than −19.5 dB, except under the conditions that the specimen thickness was 8 mm and the BV/TV ratio was 0.211 or more, thus demonstrating the high performance of the proposed method in decomposition of the fast and slow waves. The strong relationship between the phase rotation value and the value of BV/TV validated the use of the phase rotation parameter in the wave transfer function to compensate for waveform changes caused by the PLV effect. The ratio of the peak envelope amplitude of the decomposed fast wave to that of the slow wave increased monotonically with increasing BV/TV, thus demonstrating the high performance of the proposed method in estimation of the value of BV/TV in cancellous bone.

ACKNOWLEDGMENTS

This work was supported in part by the Life Science Support Program of the Terumo Foundation for Life Science and Arts, by a research grant from the Suzuken Memorial Foundation, and by KAKENHI (Grant No. 16K01431) from the Japan Society for the Promotion of Science (JSPS).

Anderson, C. C., Bauer, A. Q., Holland, M. R., Pakula, M., Laugier, P., Bretthorst, G. L., and Miller, J. G. (**2010**). "Inverse problems in cancellous bone: Estimation of the ultrasonic properties of fast and slow waves using Bayesian probability theory," J. Acoust. Soc. Am. **128**, 2940–2948.

Anderson, C. C., Marutyan, K. R., Holland, M. R., Wear, K. A., and Miller, J. G. (**2008**). "Interference between wave modes may contribute to the apparent negative dispersion observed in cancellous bone," J. Acoust. Soc. Am. **124**, 1781–1789.

Barkmann, R., Laugier, P., Moser, U., Dencks, S., Klausner, M., Padilla, F., Haïat, G., and Glüer, C. C. (**2008**). "A device for *in vivo* measurements of quantitative ultrasound variables at the human proximal femur," IEEE Trans. Ultrason. Ferroelectr. Freq. Control **55**, 1197–1204.

Bauer, A. Q., Marutyan, K. R., Holland, M. R., and Miller J. G. (**2007**). "Is the Kramers-Kronig relationship between ultrasonic attenuation and dispersion maintained in the presence of apparent losses due to phase cancellation?," J. Acoust. Soc. Am. **122**, 222–228.

Blake, G. M., and Fogelman, I. (**2007**). "Role of dual-energy x-ray absorptiometry in the diagnosis and treatment of osteoporosis," J. Clin. Densitom. **10**, 102–110.

Bouxsein, M. L., Courtney, A. C., and Haynes, W. C. (**1995**). "Ultrasound and densitometry of the calcaneus correlate with the failure loads of cadaveric femurs," Calcif. Tissue Int. **56**, 99–103.

Cardoso, L., Teboul, F., Sedel, L., Oddou, C., and Meunier, A. (**2003**). "*In vitro* acoustic waves propagation in human and bovine cancellous bone," J. Bone Miner. Res. **18**, 1803–1812.

Dencks, S., and Schmitz, G. (**2013**). "Estimation of multipath transmission parameters for quantitative ultrasound measurements of bone," IEEE Trans. Ultrason. Ferroelectr. Freq. Control **60**, 1884–1895.

Fujita, F., Mizuno, K., and Matsukawa, M. (**2013**). "An experimental study on the ultrasonic wave propagation in cancellous bone: Waveform changes during propagation," J. Acoust. Soc. Am. **134**, 4775–4781.

Genant, H. K., and Jiang, Y. (**2006**). "Advanced imaging assessment of bone quality," Ann. N.Y. Acad. Sci. **1068**, 410–428.

Groopman, A. M., Katz, J. I., Holland, M. R., Fujita, F., Matsukawa, M., Mizuno, K., Wear, K. A., and Miller, J. G. (**2015**). "Conventional, Bayesian, and Modified Prony's methods for characterizing fast and slow waves in equine cancellous bone," J. Acoust. Soc. Am. **138**, 1594–1604.

Haïat, G., Padilla, F., Peyrin, F., and Laugier, P. (**2007**). "Variation of ultrasonic parameters with microstructure and material properties of trabecular bone: A 3D model simulation," J. Bone Miner. Res. **22**, 665–674.

Haïat, G., Padilla, F., Peyrin, F., and Laugier, P. (**2008**). "Fast wave ultrasonic propagation in trabecular bone: Numerical study of the influence of porosity and structural anisotropy," J. Acoust. Soc. Am. **123**, 1694–1705.

Haïat, G., Padilla, F., Svrcekova, M., Chevalier, Y., Pahr, D., Peyrin, F., Laugier, P., and Zysset, P. (**2009**). "Relationship between ultrasonic parameters and apparent trabecular bone elastic modulus: A numerical approach," J. Biomech. **42**, 2033–2039.

Han, S., Medige, J., Davis, J., Fishkin, Z., Mihalko, W., and Ziv, I. (**1997**). "Ultrasound velocity and broadband attenuation as predictors of loadbearing capacities of human calcanei," Calcif. Tissue Int. **60**, 21–25.

Hoffman, J. J., Nelson, A. M., Holland, M. R., and Miller, J. G. (**2012**). "Cancellous bone fast and slow waves obtained with Bayesian probability theory correlate with porosity from computed tomography," J. Acoust. Soc. Am. **132**, 1830–1837.

Hosokawa, A. (**2009**). "Numerical analysis of variability in ultrasound propagation properties induced by trabecular microstructure in cancellous bone," IEEE Trans. Ultrason. Ferroelectr. Freq. Control **56**, 738–747.

Hosokawa, A. (**2010**). "Effect of porosity distribution in the propagation direction on ultrasound waves through cancellous bone," IEEE Trans. Ultrason. Ferroelectr. Freq. Control **57**, 1320–1328.

Hosokawa, A., and Otani, T. (**1997**). "Ultrasonic wave propagation in bovine cancellous bone," J. Acoust. Soc. Am. **101**, 558–562.

Hosokawa, A., and Otani, T. (**1998**). "Acoustic anisotropy in bovine cancellous bone," J. Acoust. Soc. Am. **103**, 2718–2722.

Langton, C. M., Palmer, S. B., and Porter, R. W. (**1984**). "The measurement of broadband ultrasonic attenuation in cancellous bone," Eng. Med. **13**, 89–91.

Laugier, P. (**2008**). "Instrumentation for *in vivo* ultrasonic characterization of bone strength," IEEE Trans. Ultrason. Ferroelectr. Freq. Control **55**, 1179–1196.

Laugier, P., and Haiat G., eds. (**2011**). *Bone Quantitative Ultrasound* (Springer, Dordrecht, Netherlands), pp. 1–6.

Lochmüller, E. M., Eckstein, F., Zeller, J. B., Steldinger, R., and Putz, R. (**1999**). "Comparison of quantitative ultrasound in the human calcaneus with mechanical failure loads of the hip and spine," Ultrasound Obstet. Gynecol. **14**, 125–133.

Marutyan, K. R., Bretthorst, G. L., and Miller, J. G. (**2007**). "Bayesian estimation of the underlying bone properties from mixed fast and slow mode ultrasonic signals," J. Acoust. Soc. Am. **121**, EL8–EL15.

Marutyan, K. R., Holland, M. R., and Miller, J. G. (**2006**). "Anomalous negative dispersion in bone can result from the interference of fast and slow waves," J. Acoust. Soc. Am. **120**, EL55–EL61.

Mizuno, K., Matsukawa, M., Otani, T., Laugier, P., and Padilla, F. (**2009**). "Propagation of two longitudinal waves in human cancellous bone: An *in vitro* study," J. Acoust. Soc. Am. **125**, 3460–3466.

Mizuno, K., Matsukawa, M., Otani, T., Takada, M., Mano, I., and Tsujimoto, T. (**2008**). "Effects of structural anisotropy of cancellous bone on speed of ultrasonic fast waves in the bovine femur," IEEE Trans. Ultrason. Ferroelectr. Freq. Control **55**, 1480–1487.

Mizuno, K., Somiya, H., Kubo, T., Matsukawa, M., Otani, T., and Tsujimoto, T. (**2010**). "Influence of cancellous bone microstructure on two ultrasonic wave propagations in bovine femur: An *in vitro* study," J. Acoust. Soc. Am. **128**, 3181–3189.

Nagatani, Y., Guipieri, S., Nguyen, V. H., Chappard, C., Geiger, D., Naili, S., and Haïat, G. (**2017**). "Three–dimensional simulation of quantitative ultrasound in cancellous bone using the echographic response of a metallic pin," Ultrason Imag. **39**, 295–312.

Nagatani, Y., Imaizumi, H., Fukuda, T., Matsukawa, M., Watanabe, Y., and Otani, T. (**2006**). "Applicability of finite-difference time-domain method to simulation of wave propagation in cancellous bone," Jpn. J. Appl. Phys. **45**, 7186–7190.

Nagatani, Y., Mizuno, K., and Matsukawa, M. (**2014**). "Two-wave behavior under various conditions of transition area from cancellous bone to cortical bone," Ultrasonics **54**, 1245–1250.

Nagatani, Y., Mizuno, K., Saeki, T., Matsukawa, M., Sakaguchi, T., and Hosoi, H. (**2008**). "Numerical and experimental study on the wave attenuation in bone—FDTD simulation of ultrasound propagation in cancellous bone," Ultrasonics **48**, 607–612.

Nagatani, Y., and Tachibana, R. O. (**2014**). "Multichannel instantaneous frequency analysis of ultrasound propagating in cancellous bone," J. Acoust. Soc. Am. **135**, 1197–1206.

Nelson, A. M., Hoffman, J. J., Anderson, C. C., Holland, M. R., Nagatani, Y., Mizuno, K., Matsukawa, M., and Miller, J. G. (**2011**). "Determining attenuation properties of interfering fast and slow ultrasonic waves in cancellous bone," J. Acoust. Soc. Am. **130**, 2233–2240.

Njeh, C. F., Kuo, C. W., Langton, M. M., Atrah, H. I., and Boivin, C. M. (**1997**). "Prediction of human femoral bone strength using ultrasound velocity and BMD: An *in vitro* study," Osteoporosis Int. **7**, 471–477.

O'Donnell, M., Jaynes, E., and Miller, J. G. (**1978**). "General relationships between ultrasonic attenuation and dispersion," J. Acoust. Soc. Am. **63**, 1935–1937.

Otani, T. (**2005**). "Quantitative estimation of bone density and bone quality using acoustic parameters of cancellous bone for fast and slow waves," Jpn. J. Appl. Phys. **44**, 4578–4582.

Padilla, F., and Laugier, P. (**2000**). "Phase and group velocities of fast and slow compressional waves in trabecular bone," J. Acoust. Soc. Am. **108**, 1949–1952.

Sasso, M., Haïat, G., Yamato, Y., Naili, S., and Matsukawa, M. (**2007**). "Frequency dependence of ultrasonic attenuation in bovine cortical bone: An *in vitro* study," Ultrasound Med. Biol. **33**, 1933–1942.

Sasso, M., Haïat, G., Yamato, Y., Naili, S., and Matsukawa, M. (**2008**). "Dependence of ultrasonic attenuation on bone mass and microstructure in bovine cortical bone," J. Biomech. **41**, 347–355.

Taki, H., Nagatani, Y., Matsukawa, M., Mizuno, K., and Sato T. (**2015**). "Fast characterization of two ultrasound longitudinal waves in cancellous bone using an adaptive beamforming technique," J. Acoust. Soc. Am. **137**, 1683–1692.

Taki, H., Taki, K., Sakamoto, T., Yamakawa, M., Shiina, T., Kudo, M., and Sato, T. (**2012**). "High range resolution ultrasonographic vascular imaging using frequency domain interferometry with the Capon method," IEEE Trans. Med. Imag. **31**, 417–429.

Waters, K. R., Mobley, J., and Miller, J. G. (**2005**). "Causality-imposed (Kramers-Kronig) relationships between attenuation and dispersion," IEEE Trans. Ultrason. Ferroelectr. Freq. Control **52**, 822–833.

Wear, K. A. (**2013**). "Estimation of fast and slow wave properties in cancellous bone using Prony's method and curve fitting," J. Acoust. Soc. Am. **133**, 2490–2501.

Wear, K. A. (**2014**). "Time–domain separation of interfering waves in cancellous bone using band limited deconvolution: Simulation and phantom study," J. Acoust. Soc. Am. **135**, 2102–2112.

Yamamoto, K., Yaoi, Y., Yamato, Y., Yanagitan, T., Matsukawa, M., and Yamazaki, K. (**2008**). "Ultrasonic wave properties in bone axis direction of bovine cortical bone," Jpn. J. Appl. Phys. **47**, 4096–4100.

Yamato, Y., Matsukawa, M., Yanagitani, T., Yamazaki, K., Mizukawa, H., and Nagano, A. (**2008**). "Correlation between hydroxyapatite crystallite orientation and ultrasonic wave velocities in bovine cortical bone," Calcif. Tissue Int. **82**, 162–169.